ELSEVIER

Monitoring the chemistry of self-healing by vibrational spectroscopy – current state and perspectives

Linda Zedler[1], Martin D. Hager[2,3], Ulrich S. Schubert[2,3], Matthew J. Harrington[4], Michael Schmitt[1], Jürgen Popp[1,3,5] and Benjamin Dietzek[1,3,5,*]

[1] Institute of Physical Chemistry and Abbe Center of Photonics, Friedrich Schiller University Jena, Helmholtzweg 4, 07743 Jena, Germany
[2] Institute of Organic and Macromolecular Chemistry (IOMC), Friedrich Schiller University, Humboldtstraße 10, 07743 Jena, Germany
[3] Jena Center for Soft Matter (JCSM), Friedrich Schiller University Jena, Philosophenweg 7, 07743, Jena, Germany
[4] Department of Biomaterials, Max-Planck-Institute for Colloids and Interfaces, Am Mühlenberg 1, 14424, Potsdam, Germany
[5] Leibniz Institute of Photonic Technology Jena e.V. (IPHT), Albert-Einstein-Straße 9, 07745 Jena, Germany

Self-healing materials are designed to heal damage caused by, for example, mechanical stress or aging such that the original functionality of the material is at least partially restored. Thus, self-healing materials hold great promise for prolonging the lifetime of machines, particularly those in remote locations, as well as in increasing the reliability and safety associated with functional materials in, for example, aeronautics applications. Recent material science applications of self-healing have led to an increased interest in the field and, consequently, the spectroscopic characterization of a wide range of self-healing materials with respect to their mechanical properties such as stress and strain resistance and elasticity was in the focus. However, the characterization of the chemical mechanisms underlying various self-healing processes locally within the damaged region of materials still presents a major challenge. This requires experimental techniques that work non-destructively *in situ* and are capable of revealing the chemical composition of a sample with sufficient spatial and temporal resolution without disturbing the healing process. Along these lines, vibrational spectroscopy and, in particular Raman spectroscopy, holds great promise, largely due to the high spatial resolution in the order of several hundreds of nanometers that can be obtained. This article aims to summarize the state of the art and prospective of Raman spectroscopy to contribute significant insights to the research on self-healing materials – in particular focusing on polymer and biopolymer materials.

Introduction

Self-healing materials are designed to heal damage inflicted upon them by, for example, mechanical stress or aging. The healing process results in the (partial) restoration of the material properties, such as mechanical properties, as well as other functions (*e.g.* conductivity, protection, esthetics). The basic concept of self-healing is not restricted to a single material class; it is applicable to polymers (and their composites), to concretes and asphalts, as well as to metals and ceramics [1–3]. The design of self-healing polymers and composites is often inspired by natural materials, which possess the ability to manage and repair damage encountered during their lifetime [4–8]. Biological materials have been honed through eons of evolution to perform particular functions efficiently and with economical and sustainable use of building materials, thus providing a positive role model for the development of high performance synthetic polymers and composites. The self-repair capabilities of natural systems range from the active repair of photo-damaged DNA-macromolecules to the repair of daily injuries such as small cuts, the merging of broken bones and small injuries of blood vessels up to the complete restoration of lost limbs (*e.g.* Mexican salamander (*Ambystoma mexicanum*)). While wound-healing and bone-mending are the most prominent

*Corresponding author:. Dietzek, B. (benjamin.dietzek@ipht-jena.de)

1369-7021/06/$ - see front matter http://dx.doi.org/10.1016/j.mattod.2014.01.020

examples of natural self-healing, they rely on complex cellular mechanisms, which are inherently difficult to imitate at the molecular level. Alternatively, several examples of acellular biological materials exist in which autonomic healing is intrinsic to the biopolymer itself – two of which will be discussed in detail in the following section. In man-made materials, on the other hand, the aim of self-healing is not necessarily to completely restore the chemical integrity or composition of the material, but rather to restore its overall function as defined, for example, by the stiffness of the material, its flexibility or elasticity. Through autonomic repair of damage, in particular micro-cracks, such materials are designed to operate in complex machinery (*e.g.* airplanes), in remote locations (*e.g.* tunnels) or in coatings (for a schematic of material self-healing see Fig. 1) [9,10].

Of particular interest to this article are self-healing materials based on polymers and polymer composites. Such light-weight materials are utilized nowadays in a wide range of different applications, such as protective coatings, as structural materials in aircraft construction, as well as for active materials in polymer light-emitting diodes (PLEDs) or organic solar cells. Polymers are generally considered to be less stable than other engineered materials, like steel or concrete; therefore, a potential self-healing behavior is of special interest for these materials. Self-healing mechanisms in polymers can be divided into two basic categories: (1) extrinsic self-healing and (2) intrinsic self-healing. Extrinsic self-healing depends on the activation of an incorporated healing agent upon damage and is typically based on the encapsulation of chemical cross-linkers in capsules or vascular systems embedded in

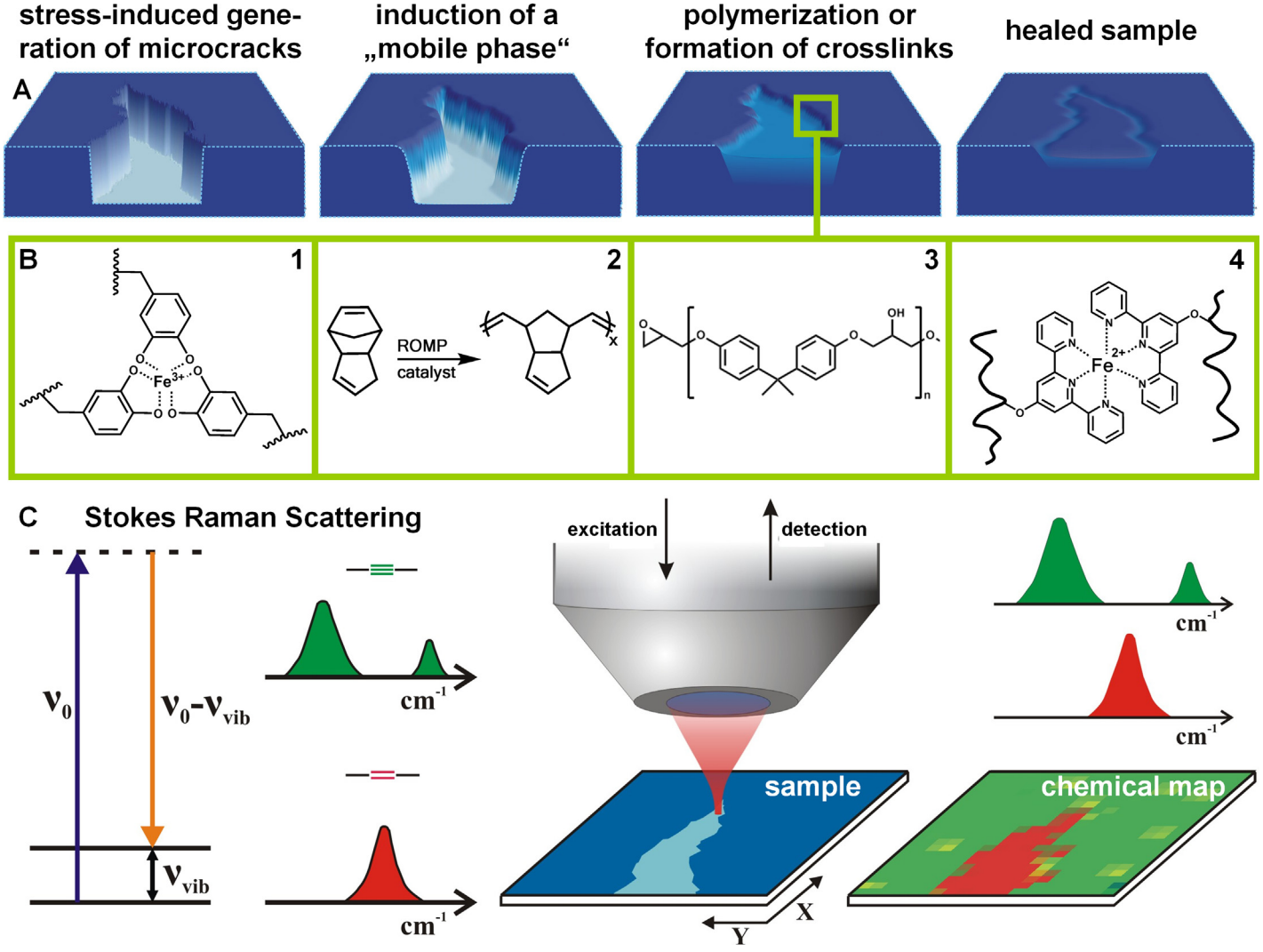

FIGURE 1

Concept of self-healings and principle of Raman microspectroscopy. (a) Upon stress induced generation of microcracks a "mobile phase" is induced, which fills the crack. Afterwards, the mobile phase solidifies by polymerization or cross-linking of polymer strands, thus restoring the mechanical properties of the material. (b) Overview of model compounds for self-healing structures based on (reversible) cross-linking processes: 1: Dopa–Fe^{3+} cross-linking by complex formation, 2: polymerization of dicyclopentadiene by ring-opening metathesis polymerization (ROMP), 3: epoxy/hardener two part adhesives, 4: Fe^{2+}-*bis*-terpyridine complexes in reversibly cross-linked polymer network by complex formation with terpyridine ligands. (c) Chemical and structural changes during cross-linking, for example, formation of linking functional structures, can be analyzed by Raman microspectroscopy. A Raman map reflects the spatial intensity distribution of a selected Raman band, for example, of the C=C stretching band (red colored), with diffraction limited, that is, sub-micrometric spatial resolution. In the color scheme red parts of the map correspond to the highest signal intensity of the C=C stretching band, while green parts refer to C≡C stretching bands. The spatial distribution of vibrational frequencies characteristic of the mobile phase and of newly formed cross-linked structures can be visualized in contrast to the bulk material to monitor the healing process.

a polymer matrix [11–14]. In contrast, intrinsic self-healing materials exhibit self-healing properties without any external ingredients, which have to be incorporated into the polymer matrix – that is, healing is inherent to the polymer itself.

One successful approach for the production of intrinsic self-healing polymers is the utilization of reversible crosslinks, that is, molecular interactions that can be reformed following damage-induced rupture. For example, such materials have been generated based on reversible covalent bond formation, for example, based on Diels–Alder and retro-Diels–Alder reactions [2,15–17], weaker non-covalent interactions, for example, hydrogen bonding [18], ionic interactions [19,20], π–π interactions [21–24], and host–guest interactions [25–27]. Additionally, the first examples of self-healing materials based on reversible metal–ligand-interactions have been demonstrated [28–30] – a concept adopted from natural materials (*e.g.* the mussel byssus), which exploit the transient properties of metal coordination bonds to achieve self-healing behaviors in harsh ocean environments (see below) [31]. Furthermore, mussel-inspired metallopolymers employing the biological metal-binding moieties (*i.e.* catechol and imidazole) have been developed and shown to exhibit moderate self-healing behavior, although the healing efficiency has not yet been explicitly quantified in a systematic way [32–34].

Irrespective of the nature of the self-healing material, from a conceptual point-of-view it is important to not only ensure that mechanical material properties are restored, but also to address the question of which molecular processes and interactions are responsible for the healing process. Elucidating the fundamental principles underlying the healing mechanism of such materials will facilitate the directed design of future generations of novel self-healing materials whose properties could be adjusted corresponding to their applications. Self-healing of materials relying on the release of healing agents requires the generation of a mobile phase (Fig. 1a) in the material because healing agents need to flow into the damage site (*i.e.* microcracking) in order to initiate the healing processes. Considering this requirement, the spatial-temporal propagation of the chemical interactions and/or molecular species responsible for self-healing must be investigated to obtain deeper insights into the underlying principles. Addressing such questions requires non-destructive experimental techniques capable of ascertaining the chemical composition of a sample with high spatial resolution (*i.e.* to monitor the local chemical composition within (micro)cracks or in the bulk material). Vibrational spectroscopy methods such as Raman scattering or IR absorption are capable of meeting these requirements in terms of chemical specificity and sensitivity to structural modifications [35–38]. In order to investigate the integrity of composite materials both depth resolved in bulk materials and at interfaces a method is required, which enables high depth penetration and microscopic spatial resolution in order to monitor chemical processes and reactions within (micro)cracks. While IR absorption micro-spectroscopy provides high signal levels, due to absorption of IR radiation, the spatial resolution and depth penetration is significantly lower than for Raman spectroscopy. This is due to the use of mid-IR radiation in the case of the IR absorption experiments and UV/vis radiation in the case of the Raman scattering experiments. Therefore, applications of IR spectroscopy to the composition and structure of self-healing materials are rare [39–43]. This review focuses in particular on Raman microspectroscopy, which combines Raman scattering with light microscopy, since it offers the sub-micron spatial resolution required to investigate self-healing processes within (micro)cracks.

The Raman effect is a consequence of the interaction of light with the electron cloud of molecules, in which a small fraction of the scattered light is shifted in wavelength as compared to the incoming light. This inelastic light scattering results from the fact that as the nuclei of molecules vibrate against each other, the electron cloud is deformed. Thus, Raman scattering can be interpreted as inelastic light scattering from vibrating molecules. Consequently, the wavelength shifts resulting from Raman scattering contain information about the characteristic molecular vibrations and, therefore, about the molecular structure. A Raman spectrum displays the intensity of inelastic light scattering at various wavelength shifts relative to the incident beam on the sample and can thus be seen as a characteristic ''spectroscopic fingerprint'' of the molecular species within the sample, allowing the identification of organic, inorganic or biological components. Furthermore, Raman spectroscopy provides important information about physical and chemical characteristics such as binding motifs, weak interactions or lone pair character since the observed Raman shifts scale with important molecular parameters like force constants or bond distances of the atoms involved in the corresponding vibration. The inter-atomic force constant determines the frequency of the vibration whereas the amount of the polarizability of the electron cloud in contrast to the atomic nuclei defines the vibrational intensities. In addition, polarization-dependent Raman spectra can deliver important information about the orientation and spatial arrangement of molecules [44]. Typical strong Raman scatterers are moieties with distributed electron clouds, such as carbon–carbon double bonds since the π-electron cloud is easily distorted in an external electric field. Bending or stretching of such bonds changes the distribution of electron density substantially, and causes a large change in the induced dipole moment. The Raman effect involves an intimate interplay between atomic positions in molecules, electron distribution and intramolecular forces. Thus, it sits at the bridgehead between structure, function and reactivity, and accordingly, Raman spectroscopy represents one of the most useful tools for obtaining information on the molecular and chemical makeup of materials, including details about the strength of the molecular bonds. Despite the many strengths of this technique, the direct assignment of Raman bands for relatively complex molecules is rather complicated. Theoretical simulations, in particular by means of density functional theory (DFT) calculations, can certainly assist to obtain a deeper understanding of the vibrational spectra of complicated molecules [45,46]. A comparison of the experimental and DFT calculated Raman spectra allows for a reliable assignment of the experimentally observed Raman bands, thus leading to a detailed understanding of the geometrical and electronic structure of the investigated molecular compounds. Due to the technical progress in the area of laser, spectrometer, optical filter- and detector development, Raman spectroscopy in combination with DFT calculations has evolved into one of the most widely used techniques in the physical and natural sciences today, providing detailed information about the structural composition of organic, inorganic and also biological molecules [36,38,47,48].

This article will review the state-of-the-art of Raman spectroscopy applied to self-healing materials by focusing on four different topical aspects. First, we discuss several cases in which Raman spectroscopy was applied to self-healing biological paradigm systems, while the remainder of the article discusses investigations of man-made polymer systems, including those based on ring-opening metathesis polymerization in the presence of a Grubbs' catalyst, as well as those based on hardening of a polymerizable epoxy resin. Finally, we discuss the potential of Raman spectroscopy to interrogate other reversible bond-formation processes, which might be implemented into self-healing materials.

Self-healing biopolymers from marine habitats – natural models for damage tolerance and repair

Extracting useful design principles from biological materials relies on understanding the material in the context of the habitat in which it evolved and performs. Organisms inhabiting the wave-swept rocky seashore, for example, face repetitive loading by powerful wave forces and abrasive water-borne particles. Thus, it is not entirely unexpected that damage tolerant materials with self-healing properties have evolved in association with marine environments. Two such materials – the mussel byssus and the egg capsules of marine whelks – are examples of tough biopolymers that dissipate large amounts of mechanical energy during cyclic loading and that exhibit autonomic and intrinsic recovery of initial properties following damage. Recently, Raman microspectroscopy was employed to probe the molecular-level structure–function relationships leading to the self-repair behavior in both materials.

Mussels are sessile organisms that anchor themselves in turbulent wave-swept habitats with protein-based biopolymeric fibers called byssal threads (Fig. 2). The extensible fibrous core of a byssal

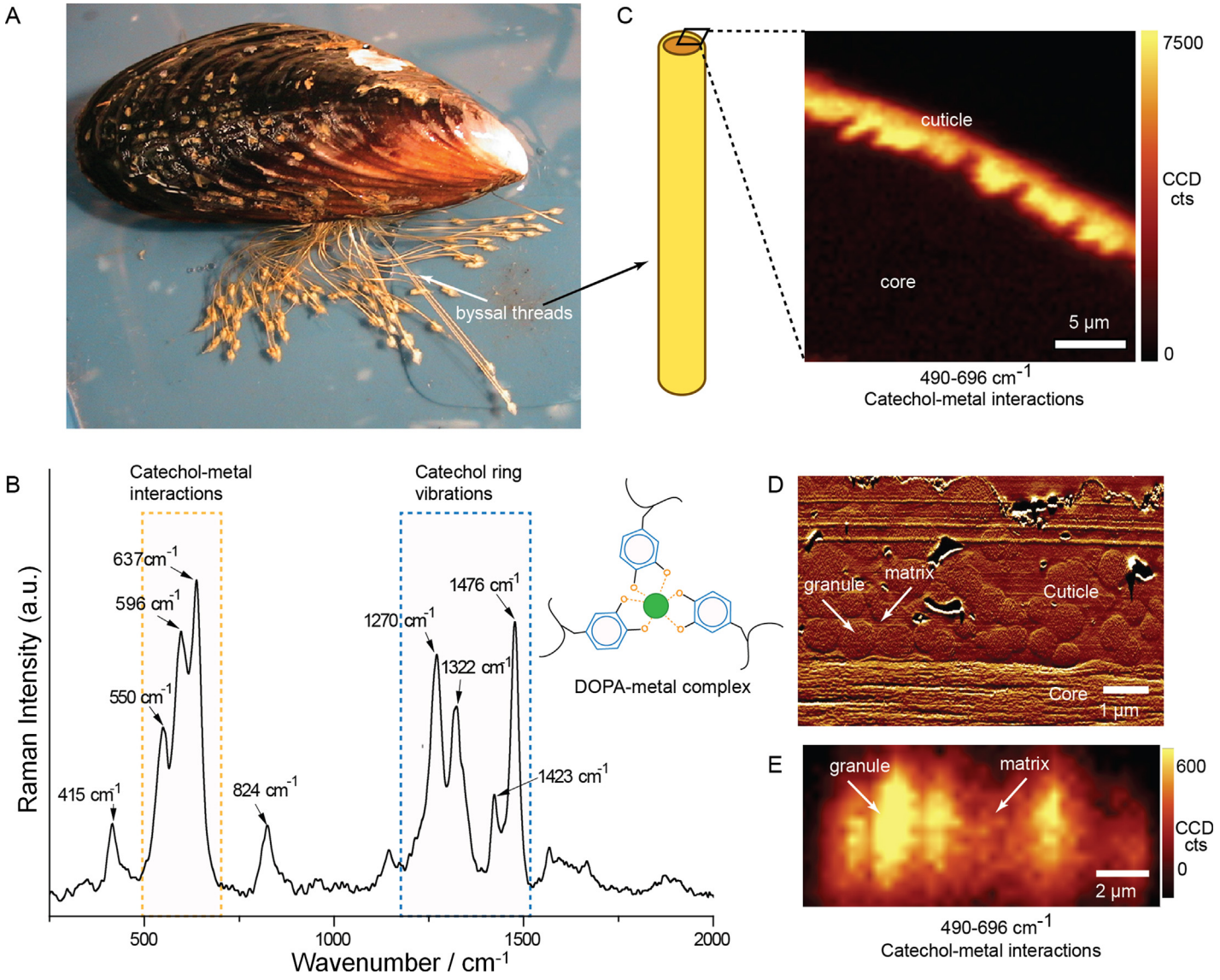

FIGURE 2

Raman evidence of metal coordination in the mussel byssus. (a) Mussels attach to hard surfaces with biopolymeric fibers called byssal threads that contain a hard, but stretchy cuticle. (b) Raman spectroscopy reveals a strong resonance signal indicative of *tris*-DOPA–metal coordination complexes, which are revealed by Raman microspectroscopy to be (c) isolated entirely within the protective cuticle and not found in the softer core of the fiber. (d) AFM image of micron-sized centers containing a high DOPA–metal complex concentration. (e) Confocal Raman microspectroscopy of thin cuticle sections reveals the chemical composition of the granular structures. Adapted from Harrington et al. with permission from AAAS [31].

thread is able to autonomically and intrinsically heal following damage from cyclic tensile deformation [49]. Additionally, the softer core is covered with a thin protective cuticle, which is remarkable in that it possesses hardness on the level of a typical epoxy, yet is extensible to up to ≈100% strain before exhibiting large crack formation [7]. Crack propagation is hindered by the granular cuticle morphology of many species (Fig. 2d), such that microcracking occurs in the soft matrix between the hard granules, which effectively distributes damage. Microcrack formation is believed to be reversible; however, until recently the molecular mechanism underlying the peculiar cuticle mechanics remained poorly characterized at the molecular level.

The byssal cuticle consists primarily of a single DOPA-rich protein, MFP-1 and is enriched with Fe^{3+} ions [50]. DOPA (3,4-dihydroxyphenylalanine) is a post-translational modification of tyrosine consisting of a catechol as a side-chain (Fig. 2b) and known for its propensity to form very stable coordination complexes with metal ions, such as Fe^{3+}. In order to specifically investigate the role of such DOPA–metal complexes in the byssal cuticle, resonance Raman spectroscopy was employed using laser excitation at 785 nm, as DOPA–metal complexes are well-known to provide a strong and distinctive resonance signal [31]. In contrast to non-resonant Raman spectroscopy, which yields integral information about the chemical composition of the whole sample, resonance Raman spectroscopy delivers information on the molecular structure of a specific chromophore within the sample, the absorption of which is in resonance with the excitation wavelength, resulting in an up to million-fold increase in the intensity of the signal over the non-resonant signal [51]. It was demonstrated that the cuticles from several different marine mussel species exhibit nearly identical resonance Raman spectra, dominated by a triplet of bands (550, 596 and 637 cm^{-1}) associated with catechol–metal interactions and four vibrational resonances between 1270 and 1476 cm^{-1}, assigned to catechol ring-breathing modes, which together identify the complexation of Fe^{3+} by DOPA units (Fig. 2b). This assignment of the characteristic vibrational modes is corroborated by control studies, in which DOPA-rich protein biopolymers isolated from marine mussels were admixed with various concentrations of Fe^{3+} ions [52,53]. In the absence of Fe^{3+} ions, the biopolymers did not show any pronounced features in the resonance Raman spectrum; however, upon addition of Fe^{3+} ions, the aforementioned vibrational triple-band in the range between 550 and 637 cm^{-1}, as well as the characteristic vibrations of the DOPA ring at higher wavenumbers emerge. Furthermore, Raman investigation of mussel-inspired PEG-DOPA polymers showed that the resonance Raman pattern associated with the DOPA–Fe^{3+} coordination is strongly pH-dependent – upon decreasing pH, the vibrational pattern indicative of the DOPA–Fe^{3+} coordination becomes increasingly structureless [32]. This was attributed to the presence of *mono*-complexed Fe^{3+} ions (one DOPA-unit coordinated to the metal in a bidentate fashion), *bis*-complexed and *tris*-complexed Fe^{3+} species, the equilibrium between which can be tuned by the pH value. Moreover, pH-tuning of the complex resulted in transitions in the mechanical integrity of the polymer ranging from a viscous solution (pH 5: mono-complexation) to a viscoelastic and self-healing hydrogel (pH 12: tris complexation).

After careful assignment of the resonance Raman bands in the mussel thread, the spatial distribution of the DOPA–metal complexes in the native material was then investigated by employing (resonance) Raman microspectroscopy coupled with a confocal microscope [31,54,55]. It was demonstrated that the catechol–metal complexes are isolated to the hard outer cuticle and absent in the softer core of the biopolymeric byssal threads and furthermore, that granules in the cuticles were local micron-sized hot spots of high DOPA–Fe^{3+} cross-link concentration in a less cross-linked surrounding matrix (Fig. 2c–e) [31]. This non-homogenous distribution of reversible cross-links suggests that the granular design of the cuticle allows damage to be localized to specific, low cross-link regions (*i.e.* the matrix), which may be healed when load is removed via reversible chemistry. From these findings, self-healing behavior based on reversible bonds is dependent not only on the presence of particular intermolecular interactions, but also on their spatial distribution, and thus, in order to understand the function of self-healing materials and to optimize their function, the morphochemistry and hierarchical structure of such systems needs to be considered. This is especially clear when considering the mechanical behavior of the unstructured mussel-inspired PEG-DOPA–Fe^{3+}-based polymers, which are not hard and stretchy like the mussel cuticle, but rather are soft and sticky hydrogels [32].

Whelks are marine gastropods that, like mussels, inhabit and reproduce in harsh seashore environments. The protective egg capsules they produce (Fig. 3a) are tough and compliant biopolymeric materials with the ability to dissipate ~50% of applied mechanical energy via mechanical yield and hysteresis [56]. Remarkably, following yield and hysteresis, which are typically associated with molecular level damage in polymeric materials, the whelk egg capsule (WEC) material instantaneously recovers its initial mechanical properties in subsequent stretching cycles (Fig. 3b) [56], a behavior reminiscent of pseudoelastic metal alloys, shape-memory polymers and certain self-healing polymers. The material design of the WEC biopolymer was investigated via traditional biochemical and materials characterization techniques, including X-ray diffraction, and it was determined that it consists of α-helical protein fibers arranged in orthogonal layers [57]. Recently, Raman-based studies have detailed the importance of reversible changes in the backbone structure of the constituent proteins in determining the self-healing behavior of the WEC.

In contrast to studying the effects of a specific chemical interaction via resonance Raman (*e.g.* DOPA–metal complexation in the mussel cuticle), traditional Raman spectroscopy was used in this case to investigate the role of protein conformational changes in the self-healing behavior of the WEC. Protein conformations, such as the α-helix and β-sheet, are organized protein backbone structures that arise from regularities or motifs in the primary amino acid sequence of a given protein. Nature makes use of regular protein conformations to stabilize three-dimensional protein topology or often as building blocks in biological materials such as hair (α-helix), spider silk (β-sheet) and collagen (triple helix). The regular conformation of an α-helix, for example, is stabilized by backbone hydrogen-bonding along the axis of the helix. While a single hydrogen-bond is weak, the effect of multiple bonds working together due to the regular structure of the α-helix makes the conformation quite stable. Proteins generally exhibit several bands in Raman spectroscopy that are strongly influenced

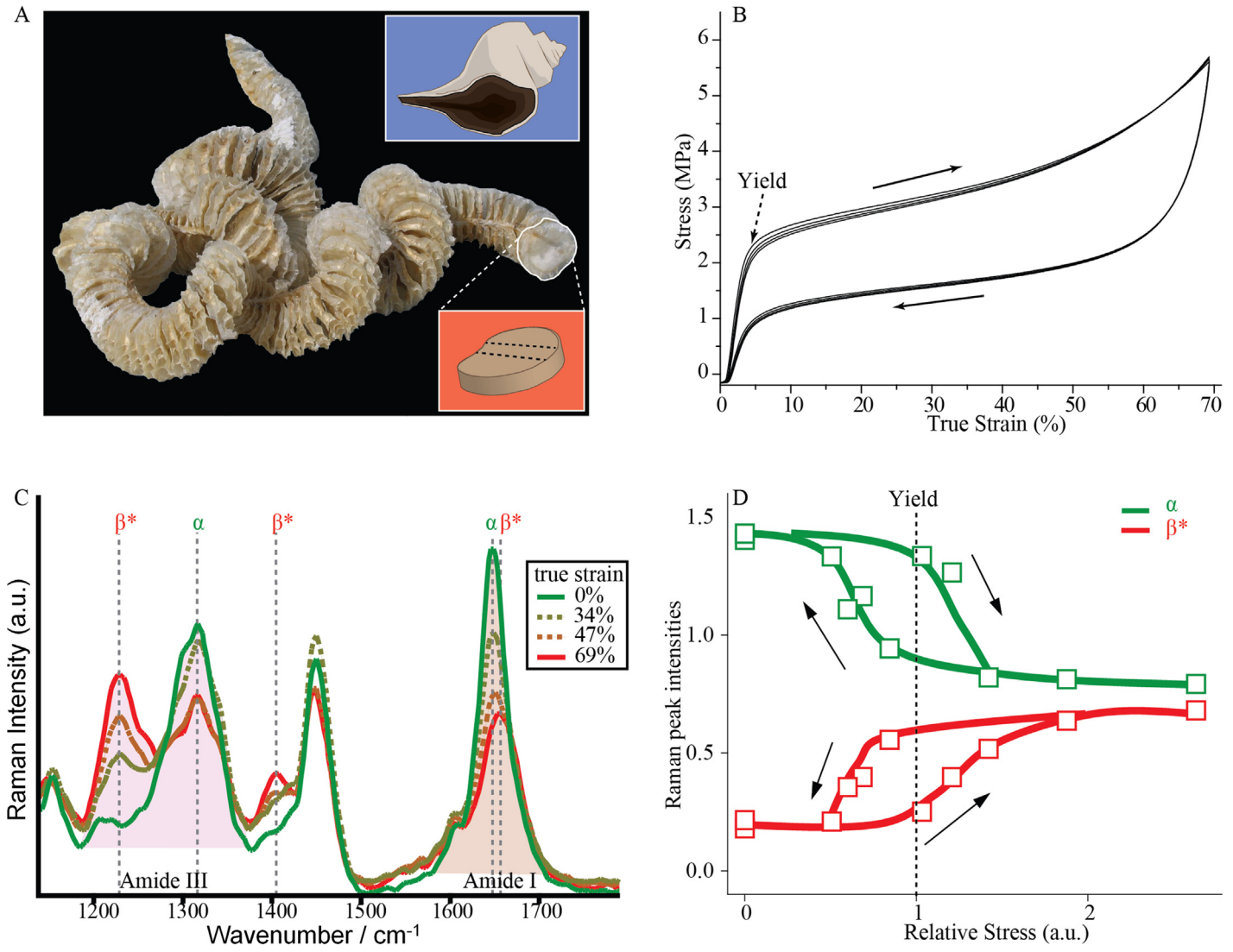

FIGURE 3

Raman spectroscopic characterization of a conformational phase transformation in the whelk egg capsule (WEC). (a) Whelks are marine gastropods that lay chains of disk-like egg capsules in the marine intertidal zone. (b) When tested in tension, the WEC biopolymer exhibits pseudoelastic mechanical behavior and recovers mechanical properties immediately following yield and hysteresis – a behavior that is reproducible over many cycles. (c) *In situ* Raman microspectroscopy during mechanical stretching reveals that the α-helical proteins that make up the egg capsule undergo a reversible transition to a more extended conformation, called β*. (d) When the intensity of the Amide III Raman peaks corresponding to the two protein conformations are plotted *vs.* relative stress (stress normalized so that yield occurs at a value of 1), a reversible structural phase transformation between the two conformations is observed. Furthermore, slow refolding of the α-helix during unloading produces a molecular hysteresis that is correlated closely with the macroscopic mechanical hysteresis. Adapted from Harrington et al. with permission from the Royal Society [58].

by the conformation of the protein backbone, the most prominent of which are the Amide I (1620–1680 cm^{-1}) and Amide III (1200–1360 cm^{-1}) bands. Consistent with earlier X-ray diffraction measurements [57], Raman spectra obtained from the fibrous layers in the WEC gave a clear signal corresponding to α-helical structure (*i.e.* Amide I centered at 1645 cm^{-1}; Amide III centered at 1316 cm^{-1}) [58]. X-ray diffraction on fully stretched samples showed that the α-helical reflections vanished, giving rise to a new structural phase [57]. In order to better understand this transformation at the level of the protein backbone structure, *in situ* Raman spectroscopy was performed on WEC during cyclic tensile testing at various strain values [58]. Results indicate a reversible conformational transition based primarily on a progressive decrease in the intensity of the α-helical Amide III band at 1316 cm^{-1} and a corresponding increase in the intensity of a new Amide III band at 1224 cm^{-1}, corresponding to an extended backbone conformation (Fig. 3c). This was also corroborated by a corresponding shift in the Amide I band and the emergence of a peak at 1400 cm^{-1}, which was assigned to C_α–H stretching that is only observed in extended conformations. Interestingly, the conversion does not occur all at once, but rather the ratio of the intensities of the two peaks gradually changes during the mechanical yield plateau (*i.e.* α-helical domains convert to extended domains progressively during loading as in a classical phase transformation) (Fig. 3c and d). Additionally, there is also a molecular-level hysteresis associated with refolding of the α-helix during mechanical unloading (*i.e.* a smaller amount of α-helix for a given load during relaxation vis-à-vis loading) that corresponds nicely with the macroscopic hysteresis observed in the material. These results were found to be consistent with results from *in situ*

small- and wide-angle X-ray diffraction measurements, which examined the structural behavior of the protein building blocks at very different length scales [58]. Thus, mechanical healing of the WEC was shown to originate from a reversible conformational phase transition in the constituent biopolymeric protein building blocks, dependent on the reversible rupture of stabilizing interactions – that is, in order to unfold α-helices, the hydrogen bonding network running along the helical axis must be ruptured allowing it to extend; however, this is evidently rapidly reformed following unloading of the material. Numerical modeling of the molecular behavior based on thermodynamic and kinetic considerations were found to be in general agreement with the Raman-based interpretation of the self-healing mechanism [58,59]. The example of the WEC again reiterates that not just the presence of a reversible bond (in this case hydrogen-bonding) is necessary for tuning self-healing behavior, but also the structural organization at various levels of hierarchy is of utmost importance.

Self-healing based on encapsulated healing agents

Many of the current generation of self-healing polymer composites are based on the fracture-induced release and subsequent curing of reactive agents in (micro)cracks, as pioneered in the seminal work by White et al. [14]. Such extrinsic healing mechanisms rely on the conversion of the mobile healing agent into a cross-linked end-product, which often possess very different Raman fingerprints. Thus, Raman spectroscopy can be used to monitor the progress of the healing process locally, which can be correlated to the degree of mechanical recovery *in situ*, revealing important chemical structure–function relationships. This method has proven useful in many instances, a handful of which are summarized below. While the examples described below are not exhaustive, they provide a suitable introduction to the field, emphasizing the potential utility of vibrational spectroscopy.

The self-healing of polymer composites was first demonstrated using ring-opening metathesis polymerization (ROMP) of

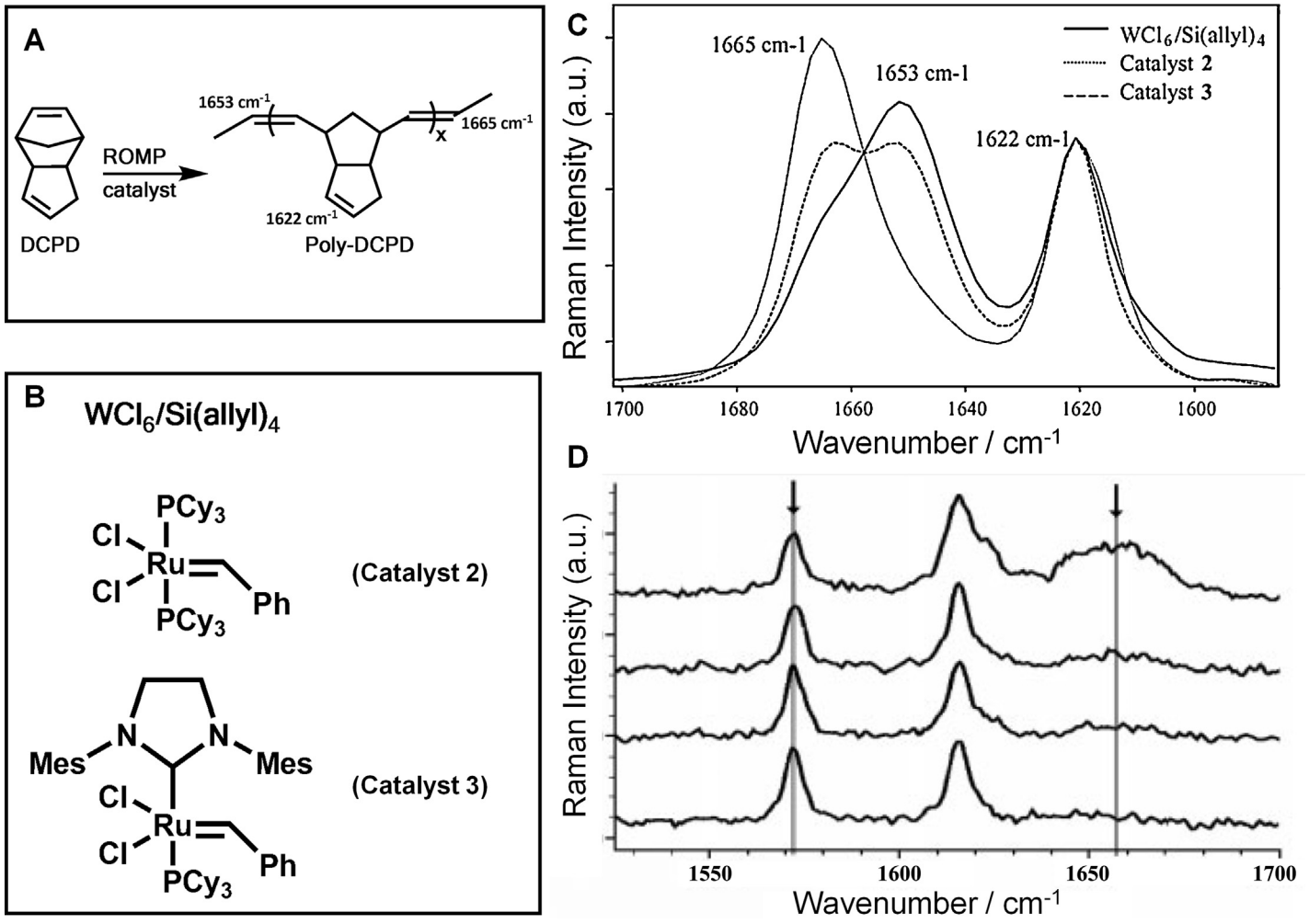

FIGURE 4

Raman spectroscopic observation of the ring-opening metathesis polymerization (ROMP). (a) ROMP of a dicyclopentadiene (DCPD). (b) Overview of Grubbs catalytic systems actuating the ROMP reaction as reported in Schaubroeck et al. [64]. (c) Raman spectra of linear poly-DCPD, illustrating the influence of the Grubbs' catalysts shown in panel B on the *trans*-/*cis*-selectivity of the cross-linking reaction. The shoulder at 1665 cm^{-1} is assigned to the stretching vibration of the *trans*-conformed aliphatic double bond. Adapted from Schaubroeck et al. with permission of Elsevier [64]. (d) Raman spectra obtained during polymerization of DCPD. An increase of the Raman mode at 1660 cm^{-1} (formation of vinyl C–C bonds) and a decrease of the Raman mode at 1568 cm^{-1} (C═C stretching vibration) with respect to the initial spectrum of DCPD confirms polymerization. Adapted from Chipara et al. with permission of Wiley [62].

dicyclopentadien (DCPD) in the presence of Grubbs' catalyst, which was monitored using *inter alia* vibrational spectroscopy to show that the ring-opened product of the DCPD polymerization (*i.e.* poly(DCPD)) was formed in the presence of Grubbs' catalyst [14,60,61]. Specifically, this was revealed by the appearance of an infrared absorption band at 965 cm^{-1} indicative of the *trans* double bond of the polymerization product. Raman spectroscopy was also used in order to monitor the material curing based of ROMP in the presence of Grubbs' catalyst, in which an increase of the Raman band at 1660 cm^{-1} associated with the vinyl C–C vibration of the polymerization product and a decrease of the Raman band at 1568 cm^{-1}, which is assigned to the C=C stretching vibration of the monomer, were used as overall indicators for the progress of the self-healing reaction (Fig. 4) [62–64]. In an extension to the often used approach of embedded microcapsules (see Fig. 5a for a schematic representation) [14,65,66], Toohey et al. developed materials that possess a microvascular network for the delivery of DCPD and Grubbs catalyst to ruptured locations within the material [67]. This approach enables multiple healing cycles of the material.

Following these initial studies, further vibrational spectroscopy investigations revealed important details concerning the mechanisms of self-healing in polymer composites based on the ROMP reaction. When following the polymerization of DCPD by non-resonant Raman spectroscopy in time-lapse experiments, clear spectroscopic changes are visible that extend far beyond the range of the vibrational bands previously discussed [63]. For example, the authors reported that the band shape of the band at around 1615 cm^{-1} changes from being rather symmetrically centered at 1612 cm^{-1} to revealing a double-peak structure (maxima at 1620 and 1612 cm^{-1}) upon completion of the polymerization reaction. Nonetheless, analysis of the time-lapse experiments focused on the prominent bands at 1568 and 1660 cm^{-1}, indicative of the reactants and the polymerization product, respectively. Within about an hour after fracturing the material, a significant rapid increase in the 1660 cm^{-1} band was observed, which is

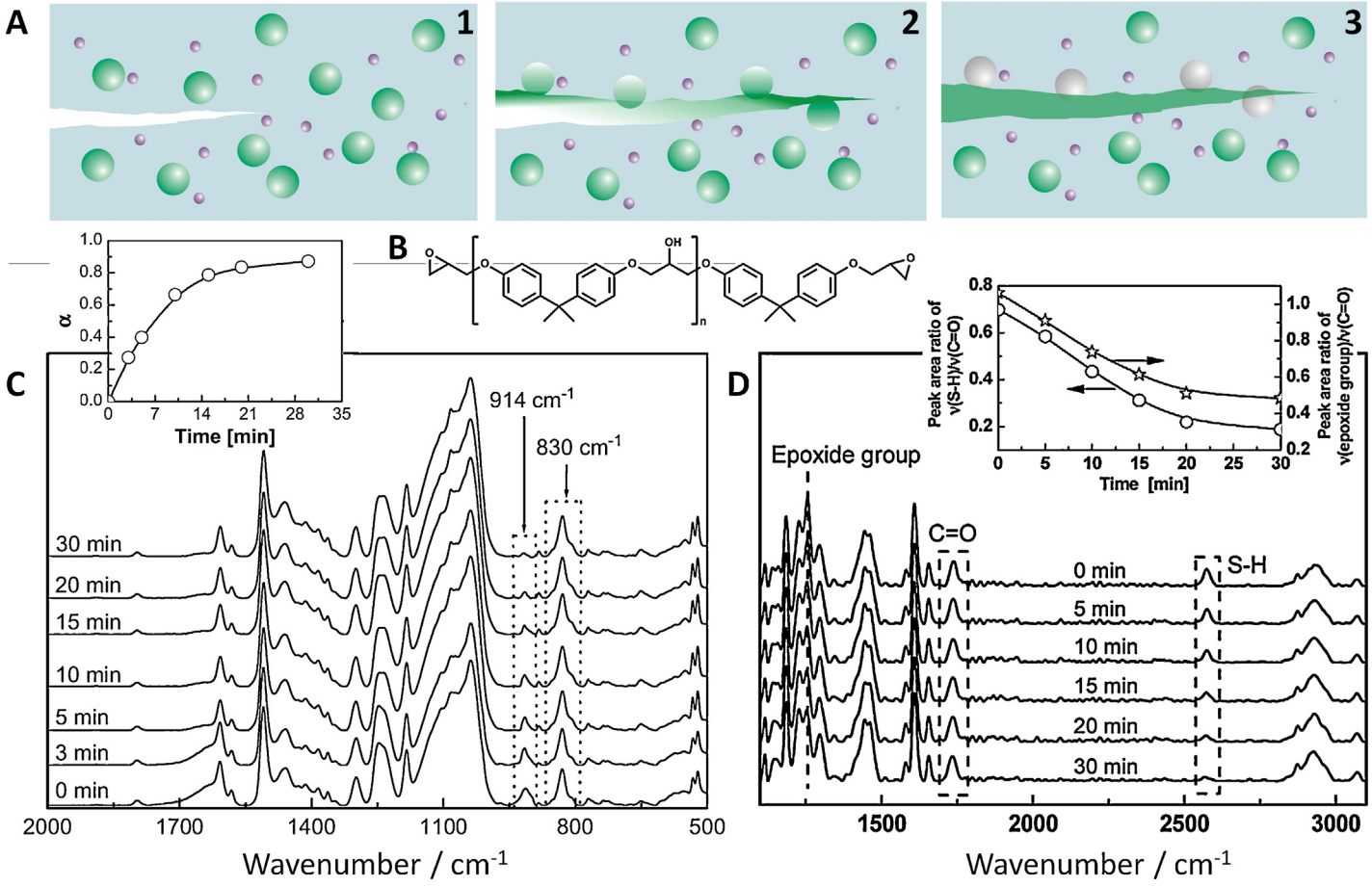

FIGURE 5

In situ time-dependent vibrational spectroscopic study of epoxy based polymerization products. (a) Principle of the autonomic self-healing process by epoxy polymerization. The matrix contains two types of microcapsules filled with epoxy prepolymer (green capsules) and a hardener, which serves as a catalyst (purple capsules) (1). When the material is damaged, the forming crack ruptures the microcapsules and the monomer is released into the crack. Upon contact with the catalyst the healing agent polymerizes (2) until the crack is mended (3). (b) Epoxy prepolymer, which reacts to an epoxy composite upon contact with a hardener. (c) FTIR spectra obtained during the curing reaction of epoxy and the hardener boron trifluoride diethyl etherate $(C_2H_5)_2O{\cdot}BF_3$ (95/5 by weight) at 20 °C (inset: reaction degree, α, as a function of time). A decrease of a characteristic peak of the epoxide group at 914 cm^{-1} confirms consumption of the epoxide within 30 min upon fracture. Adapted from Xiao et al. with permission of Elsevier [70]. (d) Monitoring the curing reaction of epoxy and mercaptane catalyzed by benzyldimethylamine using *in situ* confocal Raman spectroscopy. Observation of the decrease of characteristic Raman features of the monomers at 1256 cm^{-1} (stretching mode of epoxide group) and 2573 cm^{-1} (S–H stretching vibration of mercaptane) is consistent with a rapid curing reaction completed within 30 min. Adapted from Yuan et al. with permission of ACS [68].

correlated with rapid changes in the polymer viscosity in the same temporal window. The 1660 cm^{-1} band possesses a minor asymmetry, which the authors associate with the inhomogeneous distribution of monomeric units within the polymer strand. Furthermore, the temporal changes of the Raman spectra were correlated with measurements of the time-of-flight of a longitudinal ultrasonic wave through the polymer sample, and it was found that – due to a change in the materials modulus – the time-of-flight of a longitudinal ultrasonic wave decreases upon increase self-healing [63]. The chemical signature upon self-healing, as revealed by the Raman spectra, is completely consistent with the macroscopic material properties of the samples as reflected in the polymer viscosity or in its density and shear moduli. While the qualitative correlations of the different experimental methodologies that shed light on complementary aspects of the self-healing process are evident, the experimental results in Barnes et al. [63] lack a quantitative correlation. For instance, the fast initial rise of the Raman-band intensity associated with the polymerization product in the first minutes of the reaction are not directly mirrored in fast changes of the bulk and shear moduli of the sample. In particular, the measured ultrasonic time-of-flight data indicate no temporal changes within the first 20 min after induction of self-healing.

Furthermore, the assignment of the vibrational bands in Barnes et al. [63] was challenged by Verpoort and coworkers [64], who associated both the vibrations at 1573 and 1617 cm^{-1} to C=C stretching vibrations of the reactant monomer. In particular, the 1573 cm^{-1} was assigned to the norbornene and the 1617 cm^{-1} mode to the cyclopentene vibration of DCPD, which are shown to decrease synchronously in time-lapse Raman experiments following the self-healing reaction. Upon ring opening of the norbornene ring in the DCPD (decrease of the band at 1573 cm^{-1}), the ring tension of the cyclopentene vibration is altered, which causes the shift of the respective C=C stretching vibration from 1617 to 1622 cm^{-1}. In order to verify the origin of the asymmetry of the 1660 cm^{-1} band, Verpoort and coworkers compared the Raman spectra of the polymerization products obtained from different Grubbs' catalysts [64], which differ in their *trans*-selectivity. While the catalyst with high *trans*-selectivity caused the slightly asymmetric band shape of the C=C stretching vibration in the polymer at 1665 cm^{-1}, the less *trans*-selective catalyst produces a polymer whose Raman spectrum reveals two almost equally intense bands at 1665 and 1653 cm^{-1}, the latter of which is assigned to the *cis*-conformed double bond. Upon application of a highly *cis*-selective catalyst, that is, $WCl_6/Si(allyl)_4$, the Raman spectrum of the polymerization product reveals a dominant peak at 1653 cm^{-1} with only minor contributions from a shoulder at 1665 cm^{-1} (Fig. 4). Thus, the examples presented here further illustrate the potential of Raman spectroscopy to not only monitor temporally- and spatially-resolved changes in local chemistry, but also to monitor the stereospecificity of self-healing reactions.

In addition to ROMP reactions, other chemical approaches have been successfully integrated into microcapsule- and microvascular-based self-healing materials. For example, self-healing polymeric composites consisting of a polymerizable resin (epoxy) and a hardener as healant represent an intensively researched class of materials (see Fig. 5 for an exemplary depiction). The two-component healant is incorporated in fragile containers resembling microcapsules, which are embedded in the epoxy matrix [14]. Upon destruction of the capsules, the monomers are released into the path of the scratch and subsequent polymerization is induced by contact with an integrated catalyst in order to hamper crack propagation and to recover the original properties of the polymer (Fig. 5a) [43]. Vibrational spectroscopic techniques are quite useful for *in situ* characterization of the epoxy based polymerization products formed at the cracked surface, since polymerization involves consumption of IR- or Raman-active functional groups on the monomers that can be quantified depending on the nature of the reacting educts.

Yuan et al. [68] monitored the self-healing of an epoxy composite, consisting of microcapsules loaded with epoxy and its hardener mercaptan by means of *in situ* confocal Raman microscopy (Fig. 5d). Time-dependent Raman spectra were collected following fracture of a polymer surface possessing 2.5 wt% epoxy loaded capsules and 2.5 wt% hardener loaded capsules. With respect to the constant carbonyl stretching vibration, the simultaneous decrease of the Raman bands assigned to the S-H stretching mode of the mercaptan and the ring stretching mode of the epoxy group permitted the curing reaction between the epoxide groups and the hydrosulfide groups catalyzed by benzyldimethylamine to be monitored. The epoxy polymer is healed in less than an hour, since approximately 50% of the epoxide groups are consumed within 30 min. Similar *in situ* Raman spectroscopic studies on materials based on a polymer containing encapsulated epoxy/mercaptan healants were published three years later by the same group [69]. Time-dependent confocal Raman measurements of the extruded healing agent indicate that 70% of epoxy healant was consumed by the reaction with hydrosulfide group in the presence of the catalyst 2,4,6-tris(dimethylaminomethyl)phenol (DMP-30) within 15 min, corresponding to a threefold faster recovery of the polymer.

Xiao et al. [70] monitored curing of an epoxy resin utilizing a different hardener by means of IR spectroscopy (Fig. 5c). Advantages of this composite, which consists of epoxy and boron trifluoride etherate ($(C_2H_5)_2O{\cdot}BF_3$) loaded microcapsules as compared to the epoxy-thiol-based composites are: (1) The low catalyst concentration required to initiate the curing reaction based on cationic chain polymerization, (2) the fast curing reaction at ambient temperatures and (3) high efficiency of the healing process in terms of restoring the mechanical properties of the polymer. IR spectra reveal the consumption of epoxide by direct observation of the disappearance of a characteristic peak of the epoxide group at 914 cm^{-1}, while the IR feature at 830 cm^{-1} assigned to the phenyl ring has been used as internal standard. The results indicate that the progress of the self-healing reaction correlates with the healing efficiency – consumption of 87% of the epoxide groups within 30 min coincides well with the observed 80% recovery of impact strength of the composite in the same time window.

Zhu et al. designed multilayer microcapsule-like microreactors for application within self-healing polymers [71]. Their ''all-in-one'' system contains a liquid healing agent (*i.e.* glycidyl methacrylate) as well as a copper catalyst and the macroinitiator for the atom transfer radical polymerization. All reactive components have to be ''stored'' within different compartments (*i.e.* layers) of the final multilayer microcapsule. They performed Raman

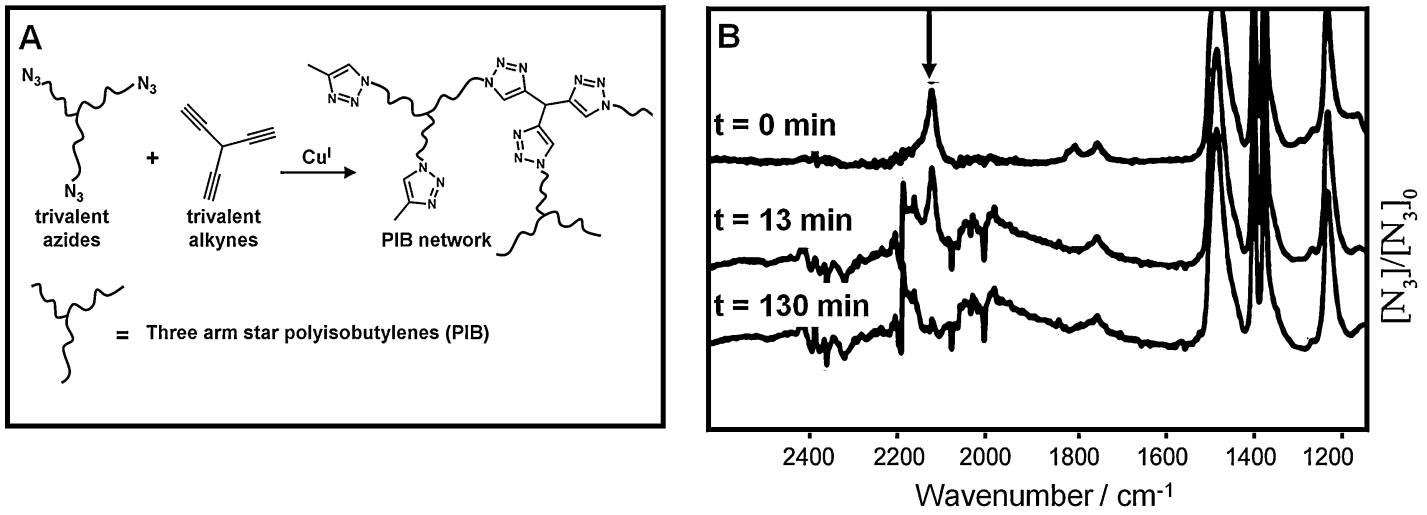

FIGURE 6

(a) "Click" reaction between trivalent polyisobutylene (PIB) azides and trivalent alkynes catalyzed by Cu(I) leads to a cross-linked polymeric network. (b) A decrease of the azide band at 2095 cm^{-1} with time during the "click" reaction measured via ATR-IR spectroscopy at 80 °C evidences complete azide conversion within 130 min. Adapted from Schunack et al. with permission of Wiley [73].

microscopy depth profiling [72] in order to investigate the local distribution of all healing agents.

Moreover, the Cu^I catalyzed click-reaction between azide and alkyne functionalized polymers shows great potential for material self-repair [74,75]. Based on existing concepts, Binder and coworkers used this reaction to crosslink polymer chains [76,77] in order to synthesize a poly(isobutylene)-based material in which microcapsules containing either low-molar mass trivalent alkynes or azide functionalized star-like poly(isobutylenes) were embedded. Additionally, a Cu^I catalyst was dispersed into the material [73]. Upon shear-force induced rupture of the microcapsules, the reactants mix with the catalyst in the polymer material, and the click-reaction leads to the healing of the crack via reformation of a polymer network. So far only AT-IR vibrational spectroscopy has been used to follow the self-healing reaction based on the temporal evolution of the azide vibration at 2095 cm^{-1} (Fig. 6). Although Raman spectroscopy has not yet been applied to these materials, it has a great potential in such studies considering that it can be applied both to bulk samples (in contrast to AT-IR) and in *in situ* studies focusing on the distribution of –C≡C– stretching vibrations even in complex biological samples as reported in a recent study on wound healing in living marine algae [78].

Prospective applications for Raman spectroscopy in monitoring reversible bond formation

Reversible temperature controlled bond formation and bond cleavage based on Diels–Alder (DA) and retro-Diels–Alder (rDA) reactions have been successfully utilized in the context of intrinsically self-healing polymers [79–81]. It was shown that the conversion of furan and maleimide to the DA product is correlated with distinct changes in the vibrational spectra, which remain clearly visible when the functional groups responsible for self-healing are diluted in a polymer matrix [82,83]. In Toncelli et al. [82] and Zeng et al. [83], the authors employed FT-IR and ATIR spectroscopy, respectively, in order to monitor the reaction and the conversion efficiency of reactants in forming the cross-linked network (Fig. 7). Due to the generally high intensity of the C=O stretching vibration in IR-absorption spectra, Zeng and coworkers based their vibrational spectroscopic investigation on the spectral-temporal shift of the IR absorption bands at 1700 and 1730 cm^{-1}, which are assigned to the carbonyl stretching vibrations of the maleimide containing crosslinking agent and to the backbone of the poly(2,5-furandimethylene succinate) (PFS), respectively, and the imide vibration of the unreacted maleimide function at 700 cm^{-1} [83]. During the healing DA reaction, which was initiated by briefly immersing the PFS in a solution of the crosslinking agent, the carbonyl vibrations remained unchanged indicating that the overall content of PFS backbone, as well as unreacted and reacted crosslinking agent stayed constant. However, the intensity of the imide vibration of the unreacted crosslinking unit decreased as a function of time revealing the progress of the healing reaction. Broekhuis and coworkers incorporated an even greater variety of IR active vibrations into their spectroscopic analysis of a cross-linked network of furan functionalized polyketones [82]. The authors compared different maleimide crosslinker concentrations (relative to the concentration of functional furan groups in the polymer) and could show that IR vibrational spectroscopy is capable of revealing the resultant chemical changes in the network, which were also clearly reflected in the mechanical properties of the samples. In addition to IR-based studies, Raman spectroscopic investigations on low-molar mass compounds, which serve as reactants in the DA/rDA chemistry have also been reported. To this end both non-resonant Raman scattering [84,85] and surface-enhanced Raman scattering [86] have been employed, proving the potential of Raman spectroscopy to be employed also for monitoring temperature-triggered DA/rDA based self-healing reactions *in situ*.

As mentioned earlier, metal–amino acid complexes based on DOPA and histidine residues are believed to play a central role in damage-tolerant biological materials. Although their bond strength lies somewhere between hydrogen bonds and covalent bonds, such complexes can be reversibly opened and closed

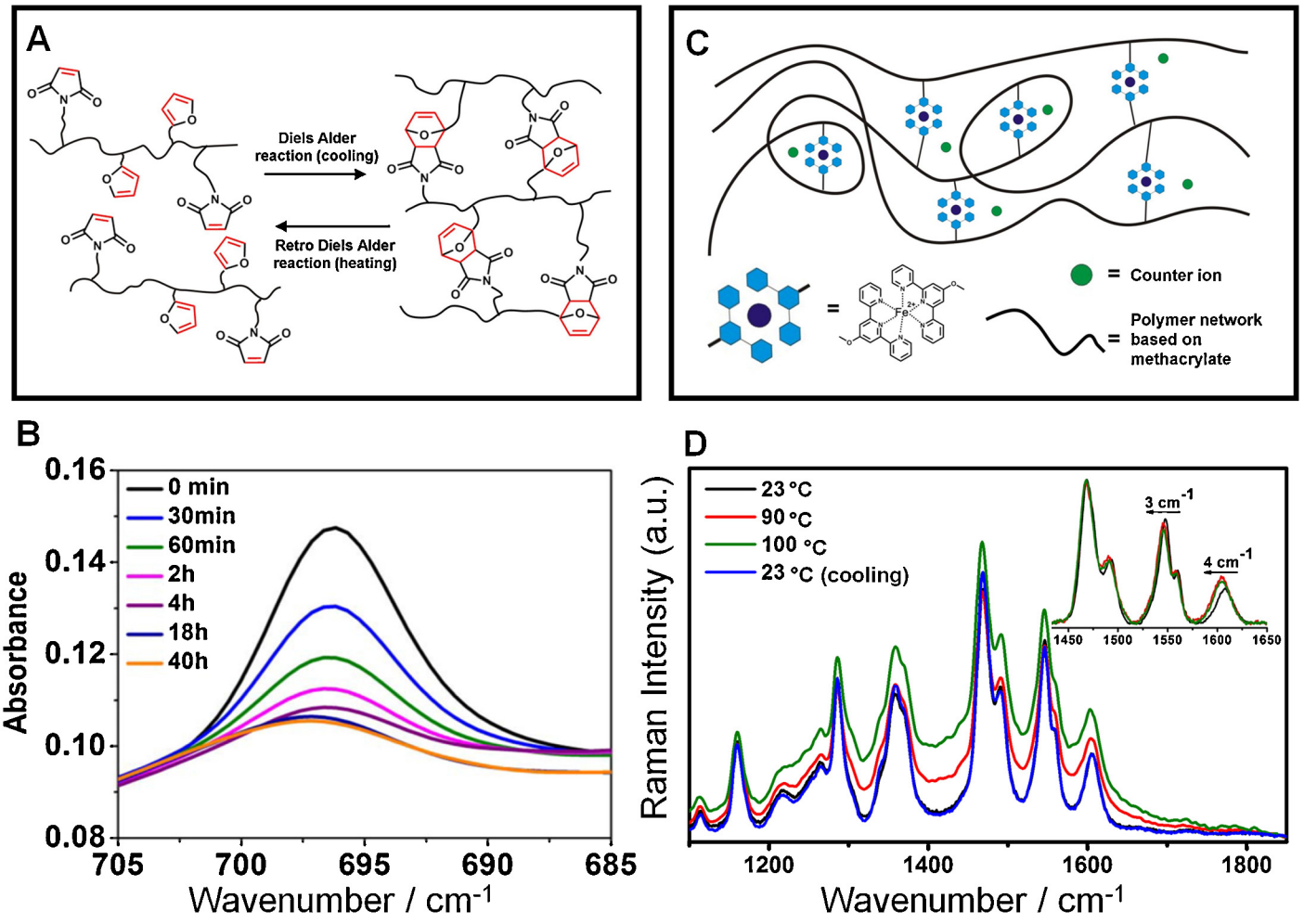

FIGURE 7

Monitoring reversible bond formation by vibrational spectroscopy. (a) Reversible Diels–Alder cycloaddition of furan and maleimide, embedded in polymer strands. (b) A progressing Diels–Alder reaction of a bio-based bis(hydroxymethyl)furan (BHF) and bismaleimide is examined by ATR-IR spectroscopy. The imide functional group is disintegrated during DA reaction. Hence, the imide peak intensity at around 700 cm^{-1} is reduced. Adapted from Zeng et al. with permission of ACS [83]. (c) Schematic drawing of a reversible cross-linked metallopolymer network based on a Fe^{2+}-terpyridine linkage. Cross-linking is based on metal–ligand interaction. (d) Terpyridine Raman modes shift to lower wavenumber upon heating the cross-linked metallopolymer indicating decomplexation of the metal–ligand structure. Adapted from Bode et al. with permission of Wiley [28].

through many cycles [87,88]. Hence, they are ideally suited to function as reversible sacrificial bonds, and this property is exploited in certain biological materials to generate self-healing behavior. For example, the large hysteresis and self-healing capabilities of the fibrous core of mussel byssal threads are – at least partially – attributed to the stabilizing effects of metal-histidine complexes [89,90]. Additionally, spider silk infiltrated with transition metal ions via atomic layer deposition (ALD) exhibits increased toughness, possibly due to the formation of coordination complexes [91]. Inspired by such findings in biomaterial paradigm systems, polymers stabilized by reversible coordination bonds based on biological ligands (*e.g.* DOPA and histidine) have been developed that show moderate self-healing behavior [32–34]. Additionally, in a promising new direction that expands beyond metal-binding ligands found in nature, bio-inspired metallopolymers based on synthetic ligands (*e.g.* between a transition metal ion and terpyridine units) have been utilized to enable self-healing. In such systems – as in the natural systems – the metal–ligand bond properties are a key factor both for the self-healing capability of the material and the overall material properties [92]. For example, factors such as bond dissociation rates [93], bond geometry and spatial organization of bonds will also exert a strong influence on mechanical properties and must therefore be considered in the rational design of new self-healing metallopolymers. Hence, the design of man-made self-healing materials based on metal coordination cross-linking, which has been realized first for the reversible connection of linear metallopolymers via metal complexation [30], will always be a compromise between optimizing self-healing behavior and tuning the material properties – for example, in hard materials the mobility of polymer-chains is low and hence the capability for self-healing, which requires individual chains to interact with each other, might be impaired. Recently, a coating based on a functional polymer bearing terpyridine functionalities in the side chains was synthesized and tested for its self-healing capabilities [28]. The self-repair of the material was initiated by increasing temperature, which was accompanied by shifts of Raman bands of about 3–4 cm^{-1} to lower wavenumbers in the spectral region between 1475 and 1650 cm^{-1}. These bands

are characteristic for the terpyridine moiety [94,95], and their reversible temperature-dependent shift indicates changes in the chemical environment of the terpyridine units during self-healing. This finding was correlated with results from small-angle X-ray scattering, which reveal that only those polymer materials, which show some short-range order, can undergo self-healing. Based on this, it was speculated that both ionic clusters in the material, which originate from the interaction of the positively charged Fe^{2+}–terpyridine complexes and the sulfate counter ion, as well as the reversibility of the metal–ligand interaction could contribute to the self-healing behavior. Interestingly, organizational order was also recently shown to be vital in the metal-dependent self-healing behavior of the fibrous core of mussel byssal threads [96].

Aside from the reversible bonds based on Diels–Alder and retro-Diels–Alder reactions and terpyridine–metal complexation mentioned above, other interactions such as pincer complexes [79,97–100], π–π-stacking interactions [21,23,101] and intermolecular hydrogen bonding [102–105] have been used to ensure reversible bond formation toward intrinsic self-healing. However, these bonds are difficult to detect using Raman spectroscopy; therefore, discussion of them lies outside the confines of this review and other methods focusing on overall material properties are more appropriate for characterization.

Conclusion and outlook

In recent years, a large number of different self-healing materials, in particular polymers and polymer composites have been developed. A great deal of effort has been spent on characterizing these materials and quantifying the healing process (*i.e.* determination of healing efficiency) [106]; however, in many cases, a thorough understanding of the underlying (molecular) mechanism is still lacking. Along these lines, chemical characterization techniques including vibrational spectroscopy, are beginning to shed light on some of these open questions. As outlined in this review, Raman spectroscopy and Raman microspectroscopy, in particular, are able to decipher the molecular mechanisms of self-healing in many polymer-based materials. In particular, the features of Raman scattering, including the ability to deduce the local chemical composition of a sample non-destructively and with a spatial resolution of less than a micrometer, have revealed detailed insights into the formation and prevalence of reversible intermolecular interactions, which are essential for self-healing. Raman (micro)spectroscopy, for example, has led to an improved understanding of the design principle of self-healing biopolymers from marine environments and of the molecular mechanisms underlying self-healing epoxies, and there is good reason to believe that this technique will continue to provide further insights into self-healing materials based on other chemistries. For example, in some materials strain-induced structural changes can lead to shifts in the Raman peaks,[107] similar to the conformational changes in protein backbone structure shown to be integral to the self-healing behavior of the WEC (Fig. 3). By this manner the local strain can be investigated, which would be otherwise only possible using certain mechanophores [108]. In this context, it has been shown that single wall carbon nanotubes (SWCNT) embedded in a polymer matrix reveal strain-induced characteristic shifts of the Raman signatures [107]. The observed shift of the G′-band at 1582 cm^{-1} is linear in the applied strain and is therefore ideally suited to examine the local strain in an epoxy resin with percolated SWCNT networks. Hence, SWCNTs embedded in (self-healing) polymer materials can be used as nanolocal Raman-spectroscopic probes for mechanochemical properties of the materials. It is expected that the general applicability of the technique will lead to deeper insights into the mechanism of self-healing polymers, in particular polymer systems based on reversible bonds/interactions. The knowledge gained can lead to a variety of novel applications, for example, in tailor-made coatings or self-healing elastomers.

Acknowledgement

The work was financially supported by the Deutsche Forschungsgemeinschaft via the Priority Program SPP 1568 ''Design and Generic Principles of Self-Healing Materials''.

References

[1] S. van der Zwaag (Ed.), Self Healing Materials – An Alternative Approach to 20 Centuries of Materials Science, Springer, Dordrecht, 2007.
[2] X. Chen, et al. Science 295 (2002) 1698.
[3] M.D. Hager, et al. Adv. Mater. 22 (2010) 5424.
[4] B.L. Smith, et al. Nature 399 (1999) 761.
[5] J. Keckes, et al. Nat. Mater. 2 (2003) 810.
[6] G.E. Fantner, et al. Nat. Mater. 4 (2005) 612.
[7] N. Holten-Andersen, et al. Nat. Mater. 6 (2007) 669.
[8] H.S. Rapoport, R.E. Shadwick, J. Exp. Biol. 210 (2007) 12.
[9] S.J. García, H.R. Fischer, S. van der Zwaag, Prog. Org. Coat. 72 (2011) 211.
[10] M.D. Hager, U.S. Schubert, Eur. Coat. J. 6 (2011) 40.
[11] A.P. Esser-Kahn, et al. Macromolecules 44 (2011) 5539.
[12] B.J. Blaiszik, et al. Annu. Rev. Mater. Res. 40 (2010) 179.
[13] A.R. Hamilton, N.R. Sottos, S.R. White, Adv. Mater. 22 (2010) 5159.
[14] S.R. White, et al. Nature 409 (2001) 794.
[15] X. Chen, et al. Macromolecules 36 (2003) 1802.
[16] J. Kötteritzsch, et al. Macromol. Chem. Phys. 214 (2013) 1636.
[17] M.J. Barthel, et al. Adv. Funct. Mater. 23 (2013) 4921.
[18] P. Cordier, et al. Nature 451 (2008) 977.
[19] S.J. Kalista, T.C. Ward, J. R. Soc. Interface 4 (2007) 405.
[20] S.J. Kalista, J.R. Pflug, R.J. Varley, Polym. Chem. 4 (2013) 4910.
[21] S. Burattini, et al. Chem. Commun. (2009) 6717.
[22] S. Burattini, et al. Faraday Discuss. 143 (2009) 251.
[23] S. Burattini, et al. Chem. Mater. 23 (2011) 6.
[24] J. Fox, et al. J. Am. Chem. Soc. 134 (2012) 5362.
[25] M. Zhang, et al. Angew. Chem. Int. Ed. 51 (2012) 7011.
[26] X. Yan, et al. Chem. Soc. Rev. 41 (2012) 6042.
[27] T. Kakuta, Y. Takashima, M. Nakahata, M. Otsubo, H. Yamaguchi, A. Harada, Adv. Mater. 25 (2013) 2849.
[28] S. Bode, et al. Adv. Mater. 25 (2013) 1634.
[29] S. Bode, et al. Polym. Chem. 4 (2013) 4966.
[30] M. Burnworth, et al. Nature 472 (2011) 334.
[31] M.J. Harrington, et al. Science 328 (2010) 216.
[32] N. Holten-Andersen, et al. Proc. Natl. Acad. Sci. U.S.A. 108 (2011) 2651.
[33] D.G. Barrett, et al. Adv. Funct. Mater. 23 (2013) 1111.
[34] D.E. Fullenkamp, et al. Macromolecules 46 (2013) 1167.
[35] I.R. Lewis, H.G.M. Edwards (Eds.), Handbook of Raman Spectroscopy: From the Research Laboratory to the Process Line, Marcel Dekker Inc., New York and Basel, 2001.
[36] B. Schrader, D. Bougeard (Eds.), Infrared and Raman Spectroscopy: Methods and Applications, VCH, Weinheim, 1995.
[37] J. Popp, A. Chiou, V.V. Tuchin, S. Heinemann (Eds.), Handbook of Biophotonics, Wiley-VCH, Weinheim, 2012.
[38] J.M. Chalmers, P.R. Griffiths (Eds.), Handbook of Vibrational Spectroscopy, John Wiley & Sons Ltd., Chichester, 2006.
[39] L. Guadagno, et al. AIP Conf. Proc. 1255 (2010) 264.
[40] G. Scheltjens, et al. J. Therm. Anal. Calorim. 105 (2011) 805.
[41] S. Neuser, V. Michaud, Polym. Chem. 4 (2013) 4993.
[42] D.V. Andreeva, et al. Adv. Mater. 20 (2008) 2789.
[43] T. Yin, et al. Compos. Sci. Technol. 67 (2007) 201.
[44] M.-E. Rousseau, et al. Biomacromolecules 5 (2004) 2247.

[45] R.G. Parr, W. Yang (Eds.), Density-Functional Theory of Atoms and Molecules, Oxford University Press, New York, 1989.
[46] P. Politzer, J.M. Seminario (Eds.), Modern Density Functional Theory: A Tool For Chemistry, Elsevier, Amsterdam, 1995.
[47] J. Popp, W. Kiefer, Fundamentals of Raman spectroscopy, in: R.A. Meyers (Ed.), Encyclopedia of Analytical Chemistry, Wiley, Chichester, 2000, pp. 13104–13142.
[48] M. Schmitt, J. Popp, J. Raman Spectrosc. 37 (2006) 20.
[49] E. Carrington, J.M. Gosline, Am. Malacol. Bull. 18 (2004) 1.
[50] C. Sun, J.H. Waite, J. Biol. Chem. 280 (2005) 39332.
[51] M. Wächtler, et al. Coord. Chem. Rev. 256 (2012) 1479.
[52] S.W. Taylor, et al. Inorg. Chem. 35 (1996) 7572.
[53] D.S. Hwang, et al. J. Biol. Chem. 285 (2010) 25850.
[54] A. Walter, et al. Analyst 135 (2010) 908.
[55] K. Grosser, et al. Biofouling 28 (2012) 687.
[56] H.S. Rapoport, R.E. Shadwick, Biomacromolecules 3 (2002) 42.
[57] A. Miserez, et al. Nat. Mater. 8 (2009) 910.
[58] M.J. Harrington, et al. J. R. Soc. Interface 9 (2012) 2911.
[59] F.D. Fischer, M.J. Harrington, P. Fratzl, New J. Phys. 15 (2013) 065004.
[60] M. Kessler, N. Sottos, S. White, Compos. A: Appl. Sci. Manuf. 34 (2003) 743.
[61] E.N. Brown, S.R. White, N.R. Sottos, Compos. Sci. Technol. 65 (2005) 2474.
[62] M.D. Chipara, et al. Polym. Adv. Technol. 20 (2009) 427.
[63] S.E. Barnes, et al. Spectrochim. Acta A: Mol. Biomol. Spectrosc. 61 (2005) 2946.
[64] D. Schaubroeck, et al. J. Mol. Catal. Chem. 254 (2006) 180.
[65] E.N. Brown, S.R. White, N.R. Sottos, J. Mater. Sci. 39 (2004) 1703.
[66] G.O. Wilson, et al. Adv. Funct. Mater. 18 (2008) 44.
[67] K.S. Toohey, et al. Nat. Mater. 6 (2007) 581.
[68] Y.C. Yuan, et al. Macromolecules 41 (2008) 5197.
[69] Y. Yuan, et al. Express Polym. Lett. 5 (2011) 47.
[70] D.S. Xiao, et al. Polymer 50 (2009) 2967.
[71] D.Y. Zhu, M.Z. Rong, M.Q. Zhang, Polymer 54 (2013) 4227.
[72] C. Hu, et al. Soft Matter 8 (2012) 4780.
[73] M. Gragert, M. Schunack, W.H. Binder, Macromol. Rapid Commun. 32 (2011) 419.
[74] V.V. Rostovtsev, et al. Angew. Chem. Int. Ed. 41 (2002) 2596.
[75] C.W. Tornøe, C. Christensen, M. Meldal, J. Org. Chem. 67 (2002) 3057.
[76] W.H. Binder, R. Sachsenhofer, Macromol. Rapid Commun. 28 (2007) 15.
[77] W.H. Binder, R. Sachsenhofer, Macromol. Rapid Commun. 29 (2008) 952.
[78] I.A. Weissflog, et al. Chembiochem 14 (2013) 727.
[79] S.D. Bergman, F. Wudl, J. Mater. Chem. 18 (2007) 41.
[80] A.M. Peterson, R.E. Jensen, G.R. Palmese, ACS Appl. Mater. Interfaces 2 (2010) 1141.
[81] P. Reutenauer, et al. Chem. Eur. J. 15 (2009) 1893.
[82] C. Toncelli, et al. Macromol. Chem. Phys. 213 (2012) 157.
[83] C. Zeng, et al. Macromolecules 46 (2013) 1794.
[84] M. Karabacak, A. Çoruh, M. Kurt, J. Mol. Struct. 892 (2008) 125.
[85] T. Kim, et al. J. Raman Spectrosc. 42 (2011) 2069.
[86] S.W. Joo, Bull. Korean Chem. Soc. 29 (2008) 1761.
[87] H. Lee, N.F. Scherer, P.B. Messersmith, Proc. Natl. Acad. Sci. U.S.A. 103 (2006) 12999.
[88] L. Schmitt, et al. Biophys. J. 78 (2000) 3275.
[89] E. Vaccaro, J.H. Waite, Biomacromolecules 2 (2001) 906.
[90] M.J. Harrington, et al. J. Struct. Biol. 167 (2009) 47.
[91] S.-M. Lee, et al. Science 324 (2009) 488.
[92] G.R. Whittell, et al. Nat. Mater. 10 (2011) 176.
[93] W.C. Yount, D.M. Loveless, S.L. Craig, Angew. Chem. Int. Ed. 44 (2005) 2746.
[94] S. Kupfer, et al. Phys. Chem. Chem. Phys. 13 (2011) 15580.
[95] M. Presselt, et al. J. Phys. Chem. C 112 (2008) 18651.
[96] S. Krauss, et al. Biomacromolecules 14 (2013) 1520.
[97] R. Dobrawa, F. Würthner, J. Polym. Sci. A: Polym. Chem. 43 (2005) 4981.
[98] H. Hofmeier, U.S. Schubert, Chem. Soc. Rev. 33 (2004) 373.
[99] P.R. Andres, U.S. Schubert, Adv. Mater. 16 (2004) 1043.
[100] A. El-ghayoury, et al. Macromolecules 36 (2003) 3955.
[101] R. Scott Lokey, B.L. Iverson, Nature 375 (1995) 303.
[102] J. Courtois, et al. Adv. Funct. Mater. 20 (2010) 1803.
[103] F. Herbst, et al. Macromolecules 43 (2010) 10006.
[104] V. Berl, et al. Chem. Eur. J. 8 (2002) 1227.
[105] S. Burattini, et al. Chem. Soc. Rev. 39 (2010) 1973.
[106] R.K. Bose, U. Lafont, J.M. Vega, S.J. Garcia, S. van der Zwaag, in: W.H. Binder (Ed.), Self-Healing Polymers, Wiley, Weinheim, 2013, pp. 335–359.
[107] A. de la Vega, et al. Compos. Sci. Technol. 71 (2011) 160.
[108] D.A. Davis, et al. Nature 459 (2009) 68.